CIRP Annals - Manufacturing Technology 70 (2021) 467–470

Contents lists available at ScienceDirect

CIRP Annals - Manufacturing Technology

journal homepage: https://www.editorialmanager.com/CIRP/default.aspx

Characterization of laser powder bed fusion surfaces for heat transfer applications

Jason C. Fox[a,*], Christopher Evans (1)[b], Kuldeep Mandloi[b]

[a] National Institute of Standards and Technology, 100 Bureau Drive, Gaithersburg, MD, 20899 USA
[b] Center for Precision Metrology, University of North Carolina at Charlotte, 9201 University City Blvd., Charlotte, NC 28223 USA

ARTICLE INFO

Article history:
Available online 11 June 2021

Keywords:
Additive manufacturing
Surface analysis
Heat transfer

ABSTRACT

Imperative to the adoption of additive manufacturing for heat transfer applications is the understanding of as-built surface texture. In this work we analyze surface height data to determine the effect of build angle. Surface data is analyzed using existing and novel techniques and results are interpreted with respect to potential impact on heat transfer efficiency. Results show that complexity in the scan strategy of the build leads to difficulties developing correlation to existing techniques. Particles are also segmented from the surface and analysis of position show relationship to surface build angle, which may create stagnation points that detriment heat transfer.

1. Introduction

Additive manufacturing (AM) is capable of producing complex parts and enables a new freedom of designs. With this freedom comes the ability to produce internal channels and features, which are not feasible with traditional manufacturing systems. This enables improvements in many applications, including heat exchanger efficiency [1]. Despite these advances there are still limitations to adoption. To optimize heat transfer, we must understand surface topographies and how they enhance or degrade heat transfer. To do this, a strong understanding of as-built surface texture and its effect on fluid flow is required.

Much of industry [2] and research [3] rely on the arithmetic average deviation from the mean line, or *Ra* (see ASME B46.1 [4] or ISO 4287 [5] for definition). It is clear, however, that *Ra* will not be enough to describe AM surface texture thoroughly [6]. Increases in surface roughness often improve heat transfer at the expense of fluid flow. Thus, both factors must be considered [1].

Work by Kandlikar *et al.* [7] investigated the effect of surface roughness on pressure drop in microchannels, suggesting the maximum profile peak height (*Rp*) and mean spacing of profile elements (*RSm*) provide better correlation to friction factor. Work by Stimpson *et al.* [8] found that in most cases increases in as-built roughness (using *Ra* values from each wall in the channel averaged together) increased friction factor; however, *Ra* varied greatly in a channel depending on build angle and correlations to *Ra* did not always hold. Thus, a more detailed understanding of the surface-texture characteristics that affect heat transfer will allow us to better optimize designs.

Thermal-fluid modeling can improve this understanding but has been limited for AM surfaces. This is likely due to the complex topographies compared to traditional manufacturing. In general, the laser powder bed fusion (LPBF) surface is expected to consist of the fully melted and re-solidified metal (e.g., weld tracks) and the partially melted powder particles (e.g., see Fig. 2a in [6] for example of both). The way in which the surface is fabricated will change the ratio of those two [6,9,10], as well as more detailed characteristics of the re-solidified surface (e.g., cracks [6], weld ripples [11], etc.). Researchers are continually developing novel segmentation methods to isolate and analyze these features individually for more detailed characterization [9,11,12].

In this work, several characterization techniques are used to better understand the effect of build angle on surface features that may influence heat transfer. Novel techniques are used to segment particles from the surface and determine the extent to which they contribute to the various analyses. Key characteristics of the surface investigated were the area scale, amplitude-wavelength content, and positions of partially-melted powder particles on the surface. The results provide functionally significant variation not captured by standard parameters available in ASME B46.1 [4] and ISO standards [5,13]. These variations are expected to affect heat exchanger efficiency that will be tested via modeling and experimentation in future work.

2. Methods

The data used in this analysis is a subset of surfaces from the publicly available dataset by Fox, 2019 [14]. Full details of the experiment setup, measurement procedure, and data handling are available in [14]. For brevity, all the same nomenclature and naming conventions used in [14] will also be used here. The data provided in [14] was captured using a focus variation microscope from artifacts built using nickel superalloy 625 (IN625). IN625 was chosen for this study as its

* Corresponding author
E-mail address: jason.fox@nist.gov (J.C. Fox).

https://doi.org/10.1016/j.cirp.2021.04.032
0007-8506/Published by Elsevier Ltd on behalf of CIRP.

corrosion resistance at high temperatures creates potential for heat transfer applications [15].

The artifacts were built in a commercially available LPBF system, an EOS M290[1] (see Fig. 2 and Fig. 5 from https://doi.org/10.6028/jres.124.023 [14]). The data selected for this analysis was from artifact STV5, which was built in the center of the build platform. Surface data from a single rib on the artifact (Rib 1), which faced toward the back of the build chamber was used. The surfaces from STV5 Rib 1, named Surf 1 through Surf 9, were built at angles of 165° to 45° in 15° increments as measured from the build plane, respectively. Thus a 90° surface (Surf 6) is vertical, below that (Surf 7 to Surf 9) are downward facing (75° to 45°), and above that (Surf 1 to Surf 5) are upward facing (165° to 105°). Table 1 in the *Spatial wavelength analysis* Section also provides surface angles. All data was leveled by subtracting a best fit mean plane with vertical residuals prior to any other analysis. Digital Gaussian filters were used and nesting indices are indicated throughout the work to document how and when data was filtered.

2.1. Spatial content

Spectral analysis is commonly performed on surface topography data. For nearly anisotropic surfaces well described by a Fourier expansion, this approach is appropriate [16]. The surfaces considered here meet neither condition, suggesting the need for alternative approaches [17]. Ignoring the phase relationship, the absolute value of amplitude averaged across the build layers, or "lay" (e.g., Fig. 1 in [18]), was calculated. This provides insight into the significant spatial periods and slopes at scales close to the peak in the area scale analyses.

2.2. Area scale analysis

Scale sensitive analysis is well described in Brown *et al.* [19] and ASME B46.1, Section 10 [4]. For this analysis, raw height data from the microscope, trimmed to a 4 mm square as discussed in [14], was imported into Mountains Maps 8.2 [20]. Since heat transfer is related to area, area analysis with rectangular tiling (i.e., "four corners") was applied to both the unfiltered surface height data and after segmentation to remove particles (described in the *Particle number, areal density, and segmentation* Section).

2.3. Particle number, areal density, and segmentation

Particle number and areal density were determined in Mountains Map after applying digital Gaussian filters with nesting indices of S-filter = 2.5 μm and L-filter = 80 μm. This L-filter was chosen as it is larger than the average particle diameter (~30 μm) and qualitatively accentuated the powder particles from the melt surface. Manual, minor modification of the threshold from the default (i.e., the peak of the histogram of heights above the mean plane) was performed to ensure delineation between powder particles and melt surface on the 45° and 165° surfaces.

Identification and segmentation of particles were performed using the following procedure: First, using the commercially available OmniSurf3D software [21], data was filtered using digital Gaussian filters, with nesting indices of S-filter = 2.5 μm and L-filter = 80 μm. Second, the areal core height (*Sk*) was calculated. Third, using MATLAB, the surface was thresholded to identify all points at a height equal to or greater than (*Sk*/2) above the mean line. This threshold was chosen because, in theory, if the particles are properly isolated by the above filters then the core roughness should consist of the melt surface and particles should be identifiable as peaks above the core roughness. This was the case for all surfaces, except the 165° surface where a threshold of *Sk* was used to eliminate bleed through of the melt surface. Fourth, the array of identified points was converted to a binary array. This binary array allows us to easily segment the surface by applying it as a mask to the desired data. For some of the analyses, the binary array was dilated by a radius of 10 pixels (i.e., 5 μm). The dilation was performed to better ensure the entire particle is isolated from the surrounding surface and is only used when stated explicitly.

3. Results and discussion

3.1. Spatial wavelength analysis

An analysis of spatial wavelengths was performed to determine if a small number of wavelengths heavily influence the surface topography. Identification of these key wavelengths could simplify modeling. While many systems used for modeling heat transfer have the capability to accept complex geometries in ".stl" or similar form, the large dynamic range of surface structure wavelengths and amplitudes makes this unreasonable to do so for AM surfaces. Even small areas (e.g., 1 mm x 1 mm) can be gigabytes in size when converted to a ".stl" format, making computation times unreasonably long without the use of high-performance computing systems. Thus, if simplifications that do not significantly affect the results of heat transfer simulations exist for AM surface, it would be a significant benefit.

Amplitude-wavelength analysis was performed using the methods described in the *Spatial content*. The staircasing distance varies based on the angle at which the surface was built (e.g., see Cabanettes Fig. 6 and Fig. 52 [10]). A 40 μm layer thickness was used so the staircasing distance on the surface is as follows in Table 1. If the "staircase" approximation applies for upward or downward looking surfaces, the Fourier transform should contain a continuum of spatial frequencies. Alternatively, if the surface is dominated by a cusp structure, a graph of the amplitude-wavelength should contain sharp peaks at harmonics of the fundamental frequency [18]. Initial analysis, presented in Fig. 1, shows neither condition.

Table 1
Theoretical staircasing distance on the surface by angle relative to the build platform.

Surface Name	Angle (°)	Staircasing Distance (μm)
Surf 1	165	154.5
Surf 2	150	80.0
Surf 3	135	56.6
Surf 4	120	46.2
Surf 5	105	41.4
Surf 6	90	40.0
Surf 7	75	41.4
Surf 8	60	46.2
Surf 9	45	56.6

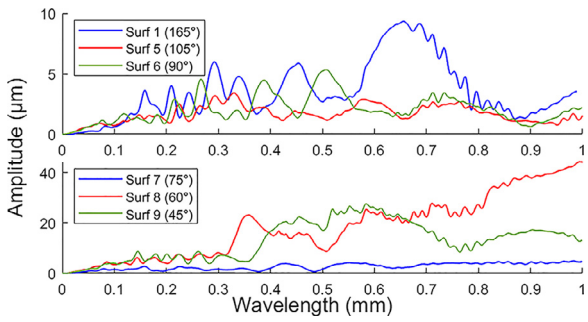

Fig. 1. Amplitude-wavelength analysis of selected surfaces (note scale change).

In this result, Surf 1 and Surf 6 (i.e., 165° and 90° surfaces) show significant "peaks" below approximately 0.7 mm at frequencies close to harmonics of 0.15 mm and 0.04 mm (e.g., the staircasing distances), respectively; however, Surf 6 also shows "peaks" near the

[1] Certain commercial equipment, instruments, or materials are identified in this paper in order to specify the experimental procedure adequately. Such identification is not intended to imply recommendation or endorsement by the National Institute of Standards and Technology, nor is it intended to imply that the materials or equipment identified are necessarily the best available for the purpose.

wavelengths not corresponding to harmonics expected. The rest of the surfaces do not appear to have any significant peaks near expected harmonics and Surf 5, Surf 7, and Surf 9 are shown in Fig. 1 as an example.

These departures from expectation could be due to a couple factors. First, the surfaces are covered with powder particles that affect the spatial wavelength analysis. Second, there is potentially a very complex interaction between the contour pass, upskin/downskin, and inskin (i.e., a pair of scan lines that make up the outermost region of the part, the region with adjusted parameters to improve "surface quality" of the part, and the bulk inner portion of the part, respectively).

In reviewing the process parameters in [14], the upskin parameters are significantly different from the inskin. Different powers and speeds were used, spacings between scan lines were different, and the pattern is a set of orthogonal scan lines on every layer as opposed to just parallel ones like the inskin. These orthogonal scan lines rotate 67° each layer, as do those in the inskin. An example of this scan strategy is shown in Fig. 2.

Additionally, the amount of upskin region on a given layer is based on a vertical distance of 120 μm (i.e., three layers) for upskin and 80 μm for downskin. This causes the horizontal distance away from the edge of a surface to vary by build angle. For the 165° surface, the distance is about 450 μm, for the 105° surface it is about 32 μm, and none for the 90°. In some situations, the upskin distance is small enough compared to the spacing between scan lines that some layers are void of upskin regions due to the 67° rotation. These could be creating inconsistencies that prevent significant peaks in the amplitude-wavelength content.

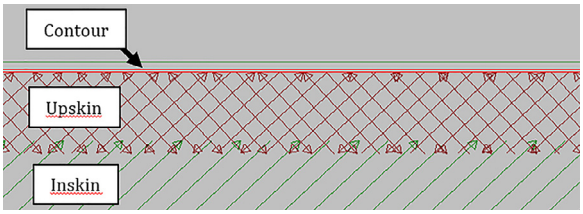

Fig. 2. Example build instructions from the EOS PSW software near a 165° surface. Bright red lines are the contour, dark red lines are the upskin, green lines are the inskin parameters. Distance between green lines in 110 μm.

3.2. Area scale analysis

Area scale analysis was performed using the methods in the *Areal scale analysis* Section. This analysis can have significant implications for thermal applications, since increases in surface area usually improve heat transfer (e.g., finned heat exchangers). Results for all surfaces are presented in Fig. 3. The relative area of Surf 8 and Surf 9 is much greater than the rest of the surfaces. Moreover, for all surfaces analyzed, there is an increase in relative area from approximately 1 μm^2 to 4 μm^2. This is likely due to the instrument transfer function of the microscope used as the slope changes at approximately four times Nyquist. There is also a rapid drop in relative area with area scale of approximately 50 μm^2 to 2500 μm^2. Area scale, for all analyses, converges to unity within parts in 10^4 for scales greater than 400 μm x 400 μm.

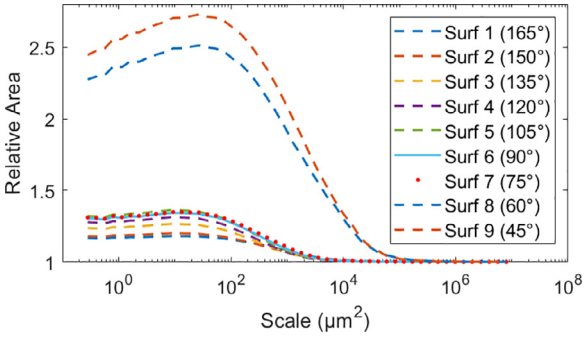

Fig. 3. Area scale analysis for all surfaces.

It is hypothesized that increases in relative area are predominately from the increasing quantity of partially melted powder particles. Increases in powder particles are expected with decreasing angle [6] and the relative area in Fig. 3 generally follows this trend. To further test this hypothesis, area scale analysis was performed on surfaces whose particles were removed using the methods in the *Particle number, areal density, and segmentation* Section. The mask was dilated by a radius of ten pixels to ensure all of the particle was removed and all non-measured points (including regions where particles were segmented out of the surface) were replaced using a bi-directional linear fill. Fig. 4 shows the comparison for surfaces Surf 1 through Surf 7 with and without particles. The results show a clear decrease in relative area, confirming the hypothesis.

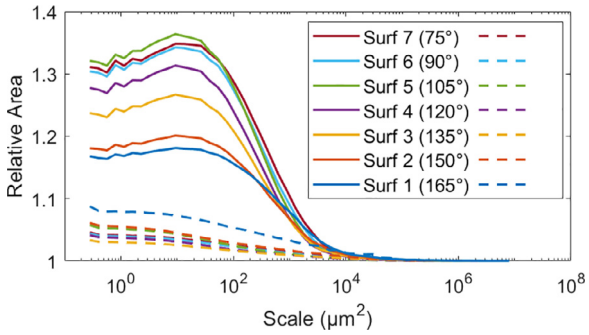

Fig. 4. Comparison of area scale for surfaces Surf 1 through Surf 7 before (solid) and after (dashed) particle removal.

3.3. Particle analysis

Using the method detailed in the *Particle number, areal density, and segmentation* Section, analysis of particles was performed. Particle count and areal density show low values for the 165° surface, level values for 150° through 75°, and higher values for 60° and 45°. Particles were also segmented from the surface to identify relationships between surface angle and particle location. For this analysis, surfaces were first filtered with nesting indices of S-filter = 2.5 μm (i.e., five times the lateral point spacing) and L-filter = 2 mm (i.e., half the lateral size of the surfaces analyzed). Second, the mask using settings detailed in the *Particle number, areal density, and segmentation* Section was used to separate particles from the remaining melt surface. The mask was not dilated in this analysis as inability to discern the particle from the surrounding surface in the dilation would skew the results. Individual particle locations in the array of height data were determined using the "regionprops()" function in MATLAB and the mean height for each particle was determined. A histogram of the mean particle heights for Surf 5, Surf 6, and Surf 7 is shown in Fig. 5.

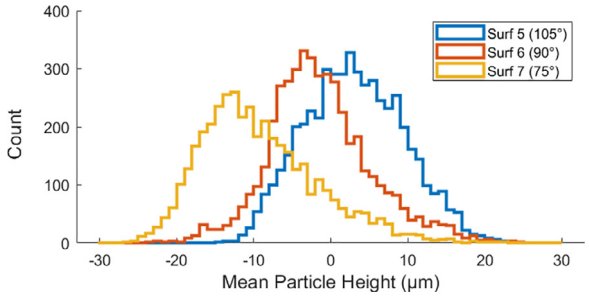

Fig. 5. Comparison of mean particle height histograms for surfaces 5, 6, and 7 (i.e., 105°, 90°, and 75° respectively).

From this figure, a trend in the mean height of powder particles is seen. The peak of the distribution shifts from above the mean plane of the surface to below as the surface angles change from upward facing, to vertical, to downward facing. This trend was also seen in Surf 1 through Surf 4 and surfaces from three other build locations in the dataset but were not included for brevity. This is a characteristic that is likely very difficult to discern with traditional parameters but may have important implications for heat transfer. As the mean particle height shifts from above the mean line to below the mean line, this indicates a shift from particles being positioned closer to the tops of weld tracks to being positioned in the valleys between weld tracks. Modeling work by the authors, which is currently being prepared for publication [22], indicates that particles positioned on the tops of weld tracks create stagnation points that inhibit heat transfer for both laminar and turbulent flow in microchannels.

4. Conclusions

Data from a publicly available dataset was analyzed with several existing and novel characterization techniques. Analysis was performed to identify more quantitative descriptions of IN625 surfaces, built via LPBF, that are anticipated to have implications for heat transfer applications. Analysis of the spatial content of the surfaces did not provide the relationship to staircasing effect that was anticipated. Two of the surfaces appeared to have peaks near the harmonics of the staircasing effect, but no surface had significant peaks at any wavelength. This could be due to the numerous powder particles or the complex scan strategy issues described in the *Spatial wavelength analysis* Section. Furthermore, the issues created by the scan strategy could be material and manufacturer dependent. With numerous machine manufacturers creating their own scan strategies, some of which are accessible and some of which are not, links of surface texture to process parameters may only hold for a very particular situation (i.e., one vendor/material/parameter set combination). Therefore, more detailed analysis of the relationship between scan strategy and the amplitude-wavelength content is suggested.

Investigation of the powder particles attached to the surfaces was performed. As expected, the quantity of attached powder particles increases with decreasing surface angle (i.e., transitions from upward facing to downward facing surfaces), but the transition was not linear and was more level for angles of 150° to 75°. Segmentation was performed using digital Gaussian filters and thresholds based on the areal parameter *Sk*. Qualitatively this analysis worked well for all but the 45° and 60° surfaces. This was likely due the large quantity of powder particles preventing adequate view of the melt surface. So while this method was quick to implement, more detailed analysis and comparison with the methods in [12] is suggested for future work.

Area scale analysis was performed on the surfaces with and without particles segmented. Results support the relationship between the quantity of powder particles and surface angle. Results also showed the significant increase in relative area caused by the presence of powder particles. Additionally, analysis of particles showed that incident angle may influence their position on the surface relative to the mean plane. This could affect heat transfer by creating stagnation points when particles are on the tops of weld tracks, as suggested by initial modeling [22]. While only a small set of surfaces (nine of the 648 available) were examined, extension to the rest of the surfaces in [14] is underway. It is anticipated that these relationships may change with changes in laser incident angle (e.g., similar to Kleszczynski *et al.* [23] and Rott *et al.* [24]).

Finally, additional modeling and experimental analysis is underway. The results of this work could have significant implications for heat transfer and fluid flow. Detailed modeling and experimental analysis should be performed to determine the extent to which these characterization techniques correlate to functional performance in heat transfer applications.

Declaration of Competing Interest

The authors declare that they have no known competing financial interests or personal relationships that could have appeared to influence the work reported in this paper.

References

[1] Zhang C, Wang S, Li J, Zhu Y, Peng T, Yang H (2020) Additive manufacturing of products with functional fluid channels: a review. *Addit Manuf* 36:101490.
[2] Todhunter LD, Leach RK, Lawes SDA, Blateyron F (2017) Industrial survey of iso surface texture parameters. *CIRP J Manuf Sci Technol* 19:84–92. Supplement C.
[3] Townsend A, Senin N, Blunt L, Leach RK, Taylor JS (2016) Surface texture metrology for metal additive manufacturing: a review. *Precis Eng* 46:34–47.
[4] ASME B46.1 (2019): Surface Texture (Surface Roughness, Waviness, and Lay), New York, NY.
[5] ISO 4287:1997. *Geometrical product specifications (GPS) – surface texture: profile method – terms*, Definitions and Surface Texture Parameters, ISOGeneva.
[6] Fox JC, Moylan SP, Lane BM (2016) Effect of process parameters on the surface roughness of overhanging structures in laser powder bed fusion additive manufacturing. *Proc CIRP, Charlotte, NC* : 131–134.
[7] Kandlikar SG, Schmitt D, Carrano AL, Taylor JB (2005) Characterization of surface roughness effects on pressure drop in single-phase flow in minichannels. *Phys Fluids* 17(10):100606.
[8] Stimpson CK, Snyder JC, Thole KA, Mongillo D (2016) Roughness effects on flow and heat transfer for additively manufactured channels. *J Turbomach* 138 (5):051008.
[9] Newton L, Senin N, Chatzivagiannis E, Smith B, Leach R (2020) Feature-based characterisation of Ti6Al4V electron beam powder bed fusion surfaces fabricated at different surface orientations. *Addit Manuf* 35:101273.
[10] Cabanettes F, Joubert A, Chardon G, Dumas V, Rech J, Grosjean C, Dimkovski Z (2018) Topography of as built surfaces generated in metal additive manufacturing: a multi scale analysis from form to roughness. *Precis Eng* 52:249–265.
[11] Senin N, Thompson A, Leach RK (2017) Feature-based characterisation of signature topography in laser powder bed fusion of metals. *Meas Sci Technol* 29(4).
[12] Newton L, Senin N, Smith B, Chatzivagiannis E, Leach R (2019) Comparison and validation of surface topography segmentation methods for feature-based characterisation of metal powder bed fusion surfaces. *Surf Topogr Metrol Prop.* 7 (4):045020.
[13] ISO 25178-2. *Geometrical product specifications (GPS) - surface texture: areal - part 2: terms*, Definitions, and Surface Texture Parameters, ISOGeneva.
[14] Fox JC (2019) Variation of surface topography in laser powder bed fusion additive manufacturing of nickel super alloy 625. *J Res Natl Inst Stand Technol* : 124.
[15] Zhang Y-C, Jiang W, Tu S-T, Zhang X-C, Ye Y-J, Wang R-Z (2018) Experimental investigation and numerical prediction on creep crack growth behavior of the solution treated inconel 625 superalloy. *Eng Fract Mech* 199:327–342.
[16] Jiang X, Scott PJ, Whitehouse DJ, Blunt L (2007) Paradigm shifts in surface metrology. Part I. Historical philosophy. *Proc R Soc Math Phys Eng Sci* 463(2085):2049–2070.
[17] Jiang X, Scott PJ, Whitehouse DJ, Blunt L (2007) Paradigm shifts in surface metrology. Part II. The current shift. *Proc R Soc Math Phys Eng Sci* 463(2085):2071–2099.
[18] Aryan H, Evans CJ, Suleski TJ (2017) On the use of ISO 10110-8 for specification of optical surfaces with mid-spatial frequency errors. *Optical design and fabrication 2017 (Freeform, IODC, OFT)*, OSA, Denver, Colorado. p. OW4B.2.
[19] Brown CA, Hansen HN, Jiang XJ, Blateyron F, Berglund J, Senin N, Bartkowiak T, Dixon B, Le Goïc G, Quinsat Y, Stemp WJ, Thompson MK, Ungar PS, Zahouani EH (2018) Multiscale analyses and characterizations of surface topographies. *CIRP Ann* 67(2):839–862.
[20] Mountains Map 8.2, 2020, Digital Surf, Besançon, France.
[21] OmniSurf3D, v1.02.002, 2019, Digital Metrology Solutions, Inc.
[22] Kuldeep Mandloi, Christopher Evans, Haris Cherukuri, Jason C. Fox, Angela Allen, David Deisenroth, Jimmie Miller, and Alkan Donmez, "A CFD analysis of the effect of build directions and surface roughness on the heat transfer and fluid flow characteristics of AM surfaces," Under Preparation.
[23] Kleszczynski S, Ladewig A, Friedberger K, zur Jacobsmühlen J, Merhof D, Witt G (2015) Position dependency of surface roughness in parts from laser beam melting systems. In: *Proceedings of the 26th international solid freeform fabrication (SFF) symposium*, Austin, TX360–370.
[24] Rott S, Ladewig A, Friedberger K, Casper J, Full M, Schleifenbaum JH (2020) Surface roughness in laser powder bed fusion – interdependency of surface orientation and laser incidence. *Addit Manuf* 36:101437.